### Title

Surface Morphing of Geometrically Patterned Active Skins




### Journal

MRS Advances, 5(14-15)

### ISSN

0272-9172



### Authors

Park, Yujin

Loh, Kenneth J



### Publication Date

2020-03-01

### DOI

10.1557/adv.2020.185

Peer reviewed

MRS Advances

# Surface Morphing of Geometrically Patterned Active Skins

Yujin Park[1] and Kenneth J. Loh[1,2,*]

[1]*Materials Science and Engineering Program, University of California San Diego*
[2]*Department of Structural Engineering, University of California San Diego*
**Corresponding author e-mail: kenloh@ucsd.edu*

*ABSTRACT*

*Nature is ripe with biological organisms that can interact with its surroundings to continuously morph their surface texture. Many attempts have been made to optimize artificial surfaces depending on operational needs; however, most of these architected materials only focus on enhancing a specific material property or functionality. This study introduces a new class of instability-induced morphable structures, herein referred to as "Active Skins", which enables on-demand, reversible, surface morphing through buckling-induced feature deployment. By taking advantage of a preconceived auxetic unit cell geometrical design, mechanical instabilities were introduced to facilitate rapid out-of-plane deformations when in-plane strains are applied. Here, these notches were introduced at judiciously chosen locations in an array of unit cells to elicit unique patterns of out-of-plane deformations to pave way for controlling bulk Active Skin behavior. These purposefully designed imperfections were employed for selectively actuating them for applications ranging from camouflage to surface morphing to soft robotic grippers.*

## INTRODUCTION

Biological organisms are able to control and display various surface topographies depending on their surroundings and for various purposes, including camouflage, locomotion, signaling, and hunting [1]. Many artificial surfaces reminiscent of these unique capabilities have been produced by mimicking and replicating the complex surface geometries of different biological systems, such as shark skins for minimizing drag coefficients [2-4], lotus leaves for self-cleaning [5], and geckos' feet for dry adhesives [6, 7], among many others. However, designing and fabricating a thin substrate into a programmable three-dimensional (3D) shape can be challenging and nontrivial [8].

One approach to achieve biomimetic morphogenesis and bio-inspired material shape morphing is by distributing the materials in a specific direction to obtain 3D shapes such as bending and rotations [9]. Furthermore, the usage of inhomogeneous and smart materials with isotropic or anisotropic properties enables the use of different external stimuli to actuate these structures and achieve shape morphing [10, 11]. Although this approach has led to controllable shapeshifting, they are only limited to certain materials. Furthermore, they do not leverage the material's overall geometrical configuration for controlling their morphology, especially as these structures change how they interact with their variable surroundings.

This study focuses on using designed imperfections to control the out-of-plane deformations of Active Skins. By leveraging a two-dimensional (2D) auxetic geometry, which exhibits zero Poisson's ratio, as the unit cell of these Active Skins, local and/or global programmable, rapid, and reversible, out-of-plane surface texture morphing can be achieved when in-plane tensile strains are applied. This paper begins with an introduction of the Active Skin, which is based on a re-entrant star pattern [12]. Many re-entrant auxetic structures have been reported, including the arrowhead, Lozenge grid, and square grid [13]. However, the re-entrant star geometry employed in this study is of a square-symmetrical configuration, which enables volumetric deformation and simplifies numerical modeling [14]. Then, the theoretical models and design methodology that are necessary to optimize accurate shapeshifting in deterministic orientations are discussed. This work concludes with experimental demonstrations and validation of Active Skin performance.

## EXPERIMENTAL AND SIMULATION DETAILS

### *Sample fabrication*

The re-entrant star geometry was modified for the Active Skins in this study (see figure 1 (a)). As shown in figure 1 (a), the outer tips of this star geometry are termed the "petal tips," while the inner tips are referred to as "sepal tips." The dimension of the star geometry was selected to have isotropic symmetry. The auxetic behavior of the star geometry relies on the angle of petal tip ($\theta_2$) to be between 30° to 40° for minimizing its Poisson's ratio [15]. Thus, the angle of the petal tip was designed to be 30° to enhance auxetic behavior. Each unit star geometry was fabricated using an Ultimaker 3+ fused deposition modelling (FDM) 3D printer. Thermoplastic polyurethane (TPU 95A) filament was used to print the design layer by layer. The geometries were first created in Autodesk Fusion 360, and then the 3D model (.stl) was uploaded to Ultimaker Cura 3.3 for prototyping. Each contour layer of the geometry was filled by alternating printing in diagonal 45º and -45º patterns to reduce the influence of infill geometry on material performance (see figure 1 (b)). The thickness of the Active Skin was 1.5 mm, and imperfections were introduced to judiciously selected locations where the depth of notches was one-third or two-thirds of the total thickness.

### *Tensile testing*

Uniaxial tensile tests were performed to characterize the mechanical response of the star geometry. The test specimens were 3D-printed with gripping tabs at both ends of the unit star geometry and loaded in a Test Resources 150R load frame equipped with a 10 N load cell. The load frame stretched the star geometry at a constant displacement rate of 2 mm/min until specimen failure, while applied load and crosshead displacements were recorded simultaneously using Keysight Benchvue. The stress-strain results were segmented into linear and nonlinear portions by employing the regression method, while the distance between petal tips were determined by image processing in MATLAB.

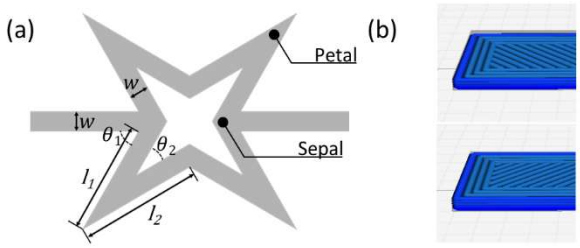


**Figure 1. (a) A unit cell Active Skin star geometry configuration is illustrated, where $l_1$ = 8.486 mm, $l_2$ = 9.353 mm, $w$ = 1.5 mm, $\theta_1$ = 60°, and $\theta_2$ = 30°. (b) A close-up view of the infill pattern of 3D-printed samples are shown.**

### *Numerical model*

A finite element model (FEM) was created to investigate stress distributions of the unit cell star geometry while being stretched. The physical size of the FEM matched the test specimens fabricated for this study. The model was meshed using 25,046 quadratic tetrahedral elements with a minimum element size of 0.125 and an average element size of 0.6709. First, the material properties of 3D-printed rectangular shaped TPU specimens were obtained through uniaxial tensile tests. Second, TPU's elastic parameters were determined by applying a nonlinear least-squares fit to the raw tensile testing data (which will be described in detail below). Then, these mechanical properties were adopted in a COMSOL hyperelastic model for calculating the nonlinear mechanical behavior of the FEM, as well as the deformation mechanism of the star geometry under uniaxial strains. Finally, it was assumed that one end of the structure was affixed, and stress was induced on the opposite end to stretch the structures by 15 mm. An auxiliary sweep was performed to enhance convergence.

## RESULTS AND DISCUSSION

### *Material parameters for FEM*

Unlike conventional bulk materials, the properties of 3D-printed samples largely depend on their fabrication parameters. Therefore, this necessitates determining the mechanical properties of 3D-printed TPU Active Skins. Figure 2 (a) plots stress ($\sigma$) versus stretch ($\lambda$), which were computed using the displacement and applied force measurements acquired during tensile testing of rectangular TPU specimens:

$$\sigma = \frac{F}{A}[MPa] \quad (1)$$

$$\lambda = 1 + \varepsilon \quad (2)$$

where $F$ is applied force, $A$ is the cross-sectional area of the specimen, and $\varepsilon$ is applied strain.

TPU was assumed to be incompressible and hyperelastic. For all elastic models, strain energy density, $\Psi$, can be stated as a function of principal stretches $\lambda_a$, where the subscript $a$ corresponds to the direction in 3D Cartesian space (*i.e.*, $a$ is 1, 2, or 3). The first Piola-Kirchhoff stress ($P_a$) for isotropic incompressible materials is:

$$P_a(\lambda) = -\frac{1}{\lambda_a}p + \frac{\partial \Psi}{\partial \lambda_a} \quad (3)$$

where an arbitrary scalar parameter ($p$) is determined from uniaxial tension, $P_1=\sigma$, and $P_2=P_3=0$ [16]. The first Piola Kirchhoff stress can be expressed using the first and second principal invariants of deformation, where $I_1$ is ($\lambda_1^2+\lambda_2^2+\lambda_3^2$), and $I_2$ is ($\lambda_1^2\lambda_2^2+\lambda_2^2\lambda_3^2+\lambda_3^2\lambda_1^2$). The strain energy for the Mooney-Rivlin model ($\Psi$) is also expressed as follows, where $\mu_1$ and $\mu_2$ are the two material parameters:

$$\sigma(\lambda) = 2\left(\lambda - \frac{1}{\lambda^2}\right)\frac{\partial \Psi}{\partial I_1} + 2\left(1 - \frac{1}{\lambda^3}\right)\frac{\partial \Psi}{\partial I_2} \quad (4)$$

$$\Psi(I_1, I_2) = \frac{\mu_1}{2}(I_1 - 3) + \frac{\mu_2}{2}(I_2 - 3) \quad (5)$$

By combining equations (4) and (5), the principle Piola-Kirchhoff stress takes the form:

$$P(\lambda) = \mu_1\left(\lambda - \frac{1}{\lambda^2}\right) + \mu_2\left(1 - \frac{1}{\lambda^3}\right) \quad (6)$$

A nonlinear least-squares method was used to fit equation (6) to the TPU tensile testing data. The results are shown in figure 2 (b), and the material properties and the two Mooney-Rivlin parameters are listed in Table 1. These material parameters were used for in the COMSOL FEM to ascertain the deformation mechanism of the Active Skin unit cell.

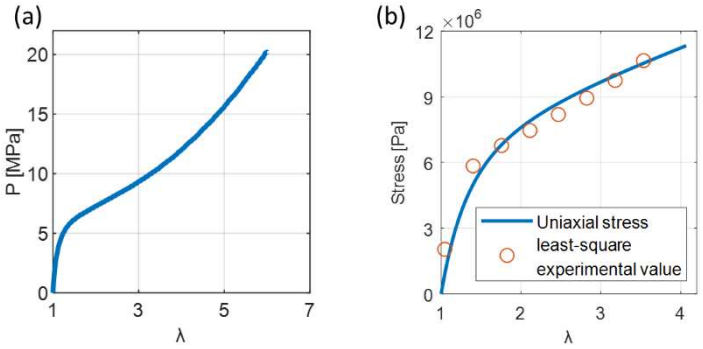


**Figure 2. (a) Stress (σ) and stretch (λ) for 3D printed TPU coupon were obtained through uniaxial tensile tests. (b) Experimental data and fitted Mooney-Rivlin model of 3D printed TPU coupon are compared**

Table 1. Material parameters of the 3D-printed TPU coupon

| | |
|---|---|
| **$\mu_1$ [MPa]** | 1.365 |
| **$\mu_2$ [MPa]** | 5.951 |
| **ρ (density) [kg/m$^3$]** | 1,200 |

## *Geometrical instability*

The deformation mechanism of a unit cell Active Skin geometry under uniaxial tensile strain is illustrated in figure 3. The stress-strain result shows that its mechanical response is nonlinear. In addition, images taken during the tensile testing and the stress distribution results from FEM analyses, corresponding to the various points marked in the stress-strain plot, are depicted together to characterize the deformation process. The Active Skin specimen used for tensile testing was 1.5 mm thick, which is the same as its width (see *w* in figure 1 (a)) to harvest buckling-induced instability of the thin substrate.

Analysis of the stress-strain plot shown in figure 3 shows that, during the initial stage of loading, linear response was observed. The Active Skin exhibits in-plane auxetic behavior, which means the distance between sepal tips (DBS) increased, while the distance between petal tips (DBP) remained constant. The stress distribution result for point A confirms that the movement of the sepal tips generated localized compression in the lateral elements right next to the sepal tips as $\theta_1$ was increased. Once $\theta_1$ reached 90º, the stress-strain curve exhibited nonlinearity, and the compressive stresses induced out-of-plane deformations of the sepal and petal tips (*i.e.*, at the end of point A). This point coincides with the critical buckling point of the star geometry, where out-of-plane deformations began.

Nonlinear behavior transitions to linear when the ends of the sepal tips and petal tips are aligned (point B). During applied in-plane tensile strains to the unit cell, stress was concentrated not only near the two sepal tips, as was previously mentioned, but also near the four petal tips where the slender elements began to buckle outwards. Out-of-plane movement was enlarged through the seesaw-like behavior of the petal and sepal tips, since they always buckled in opposite directions and pushed each other. Thus, the Active Skin reached its full-out-of-plane deformation at point C when DBP was at its minimum. After point C, DBP increased again, and the stress-strain curve became inelastic with plastic deformation observed. Overall, when applied strains were released, the Active Skins could return to its pristine flat orientation.

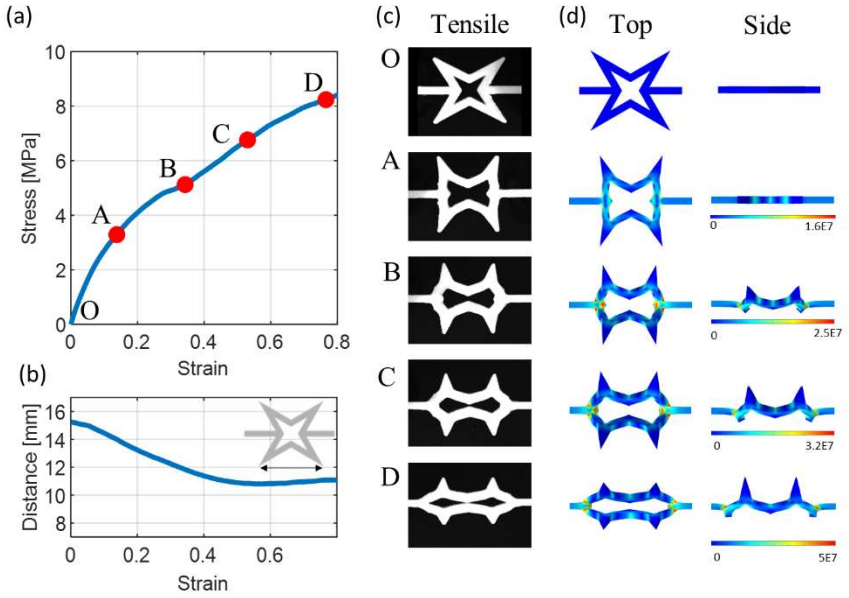


**Figure 3. (a) The mechanical response of unit cell star geometries subjected to applied uniaxial tension is plotted. (b) Images taken during the tensile test and (c) stress distribution results from COMSOL FEM results that correspond to the labeled points in (a) are shown.**

The instability of the star geometry could be magnified when substrate thickness was reduced, which means that the Active Skin produces out-of-plane deformations in response lower magnitudes of applied strains and stresses. However, since these slender elements are susceptible to extrinsic factors, thin Active Skins could deploy in random buckling directions, which is undesirable for surface morphing applications where precise

control is needed. Figure 4 (a) shows the critical locations where stresses are concentrated during out-of-plane deformations. These same locations were selected for introducing geometrical imperfections or notches to the Active Skins. The notches colored in red in figure 4 (a) would shift the neutral axis downwards, which effectively concentrated mechanical instabilities towards the desired direction. On the other hand, the notches in blue were introduced to facilitate bending.

The mechanical response of a notched Active Skin is depicted in figure 4 (b), and the points that segregate the deformation stages are also marked. The height-to-thickness ratio ($h/t$) was varied and selected as the parameter to evaluate the role of notch depth in affecting the Active Skin's critical buckling point. Figure 4 (b) shows that Active Skins with deeper notches ($h/t$=2/3) were energetically favorable in that they required a significantly lower critical buckling stress and strain to achieve pattern deployment. Moreover, figures 4 (c) and (d) show that stress is effectively concentrated only at the notches, which facilitates easier bending of the petal tips. It can also be verified from the images taken during loading that deeper notches allowed for reaching the minimum DBP at lower magnitudes of applied strains and stresses (*i.e.*, points $C_2$ versus $C_1$). Overall, this work demonstrated that designed imperfections enabled better control of the directionality of out-of-plane deformations of the star pattern. Furthermore, patterns with deeper notches needed lower critical buckling stresses and strains for triggering deployment of petal and sepal tips.

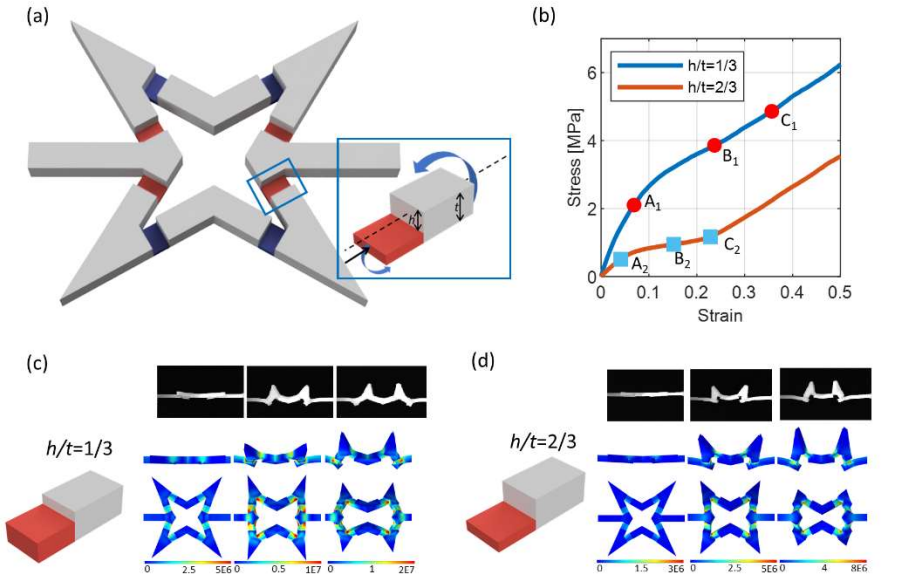


**Figure 4. (a) A rendering of the Active Skin with purposefully implemented notches is illustrated. The notches shift the neutral axis down locally and promote localized bending moments to facilitate directionally dependent buckling when strained. (b) The mechanical responses of notched Active Skins were characterized. Images of Active Skins with *h/t* of (c) 1/3 and (d) 2/3 strained in uniaxial tension are presented. The corresponding stress distributions from COMSOL FEM are also shown.**

## CONCLUSIONS

This paper demonstrated that Active Skins subjected to in-plane tensile strains could generate out-of-plane deformations into a programmable 3D shape, and the results were compared with finite element analysis. The Active Skins were designed based on a preconceived auxetic geometry, and they were 3D-printed using TPU. Unlike conventional shapeshifting approaches, which were limited to certain materials, the Active Skin geometrical design approach enables the possibility of using diverse materials for achieving surface morphing. Tensile tests were performed to analyze the star geometry's mechanical behavior, and the results were compared with COMSOL FEM results. During the deformation process, stress was concentrated on the lateral elements next to the sepal tips. and this compressive stress leads to the buckling of sepal and petal tips. The critical locations for geometrical imperfections and their role in facilitating the deployment of surface features in a controlled manner were also verified by analyzing the stress distribution results from FEM. By introducing imperfections in these unit cell star geometries, the stress generated during applied uniaxial tension concentrated at the notches, which facilitated and reduced the energy required to trigger out-of-plane pattern deployment. Overall, this study showed that Active Skins can be programmed to achieve rapid, reversible, and on-demand surface feature deployment, which can be leveraged for the structure to interact with its variable surroundings.

## References


[1] A. Rafsanjani, Y. R. Zhang, B. Y. Liu, S. M. Rubinstein, and K. Bertoldi, "Kirigami skins make a simple soft actuator crawl," (in English), *Science Robotics,* vol. 3, no. 15, Feb 21 2018.

[2] A. G. Domel, M. Saadat, J. C. Weaver, H. Haj-Hariri, K. Bertoldi, and G. V. Lauder, "Shark skin-inspired designs that improve aerodynamic performance," *J R Soc Interface,* vol. 15, no. 139, Feb 2018.

[3] B. Dean and B. Bhushan, "Shark-skin surfaces for fluid-drag reduction in turbulent flow: a review," *Philos Trans A Math Phys Eng Sci,* vol. 368, no. 1929, pp. 4775-806, Oct 28 2010.

[4] R. Garcia-Mayoral and J. Jimenez, "Drag reduction by riblets," *Philos Trans A Math Phys Eng Sci,* vol. 369, no. 1940, pp. 1412-27, Apr 13 2011.

[5] B. Bhushan and Y. C. Jung, "Natural and biomimetic artificial surfaces for superhydrophobicity, self-cleaning, low adhesion, and drag reduction," *Progress in Materials Science,* vol. 56, no. 1, pp. 1-108, 2011.

[6] H. Gao, X. Wang, H. Yao, S. Gorb, and E. Arzt, "Mechanics of hierarchical adhesion structures of geckos," *Mechanics of Materials,* vol. 37, no. 2-3, pp. 275-285, 2005.

[7] S. Das *et al.*, "Stick-slip friction of gecko-mimetic flaps on smooth and rough surfaces," *J R Soc Interface,* vol. 12, no. 104, Mar 6 2015.

[8] E. Siefert, E. Reyssat, J. Bico, and B. Roman, "Bio-inspired pneumatic shape-morphing elastomers," *Nat Mater,* vol. 18, no. 1, pp. 24-28, Jan 2019.

[9] A. M. Abdullah, X. Li, P. V. Braun, J. A. Rogers, and K. J. Hsia, "Self-Folded Gripper-Like Architectures from Stimuli-Responsive Bilayers," *Adv Mater,* vol. 30, no. 31, p. e1801669, Aug 2018.

[10] Y. Mao *et al.*, "3D Printed Reversible Shape Changing Components with Stimuli Responsive Materials," *Sci Rep,* vol. 6, p. 24761, Apr 25 2016.

[11] L. Ionov, "Hydrogel-based actuators: possibilities and limitations," *Materials Today,* vol. 17, no. 10, pp. 494-503, 2014.

[12] Y. Park, G. Vella, and K. J. Loh, "Bio-Inspired Active Skins for Surface Morphing," *Scientific Reports,* vol. 9, no. 1, p. 18609, 2019/12/09 2019.

[13] H. M. A. Kolken and A. A. Zadpoor, "Auxetic mechanical metamaterials," *RSC Advances,* vol. 7, no. 9, pp. 5111-5129, 2017.

[14] M. Chen, H. Jiang, H. Zhang, D. Li, and Y. Wang, "Design of an acoustic superlens using single-phase metamaterials with a star-shaped lattice structure," *Sci Rep,* vol. 8, no. 1, p. 1861, Jan 30 2018.

[15] V. H. Carneiro, H. Puga, and J. Meireles, "Analysis of the geometrical dependence of auxetic behavior in reentrant structures by finite elements," *Acta Mechanica Sinica,* vol. 32, no. 2, pp. 295-300, 2015.
[16] G. Marckmann and E. Verron, "Comparison of hyperelastic models for rubber-like materials," *Rubber chemistry and technology,* vol. 79, no. 5, pp. 835-858, 2006.